Distribution Category:
Energy Conversion
(UC-93)

ANL-81-67

ANL--81-67

DE82 021146

ARGONNE NATIONAL LABORATORY
9700 South Cass Avenue
Argonne, Illinois 60439

ADVANCED-FUEL-CELL DEVELOPMENT

Progress Report for
October-December 1980

by

R. D. Pierce, R. M. Arons,* J. T. Dusek,* A. V. Fraioli,
G. H. Kucera, J. W. Sim, and J. L. Smith

Chemical Engineering Division

June 1982

Previous reports in this series

ANL-80-33	October-December 1979
ANL-80-67	January-March 1980
ANL-80-98	April-June 1980
ANL-81-16	July-September 1980

*Materials Science Division, ANL.

TABLE OF CONTENTS

LIST OF FIGURES

LIST OF TABLES

ADVANCED FUEL CELL DEVELOPMENT

Progress Report for
October-December 1980

by

R. D. Pierce, R. M. Arons, J. T. Dusek, A. V. Fraioli,
G. H. Kucera, J. W. Sim, and J. L. Smith

ABSTRACT

This report describes the fuel cell research and development activities at Argonne National Laboratory (ANL) during the period October through December 1980. These efforts have been directed toward (1) developing alternative concepts for components of molten carbonate fuel cells and (2) improving understanding of component behavior.

The principal focus has been on development of γ-$LiAlO_2$ sinters as electrolyte structures. Green bodies were prepared by tape casting and then sintering β-$LiAlO_2$; this has produced γ-$LiAlO_2$ sinters of 69% porosity. In addition, a cathode prepared by sintering lithiated nickel oxide was tested in a 10-cm square cell. Although the bimodal pore distribution in the cathode successfully provided agglomerates flooded with electrolyte and open pores for gas passage, the cathode dimensional variations prevented good contact with the tile, which was stiffer than normal. The tile was prepared using an improved synthesis procedure, which resulted in high-surface-area γ-$LiAlO_2$ particles; but, because the carbonate content was the same as used in previous tests, the tile was less compliant. The cell had excellent seals because dimensional changes associated with in situ cathode reactions were eliminated.

SUMMARY

Development of Electrolyte Structures

Preparation of $LiAlO_2$ for Sintered Structures

Four batches of β-$LiAlO_2$ were synthesized by a process involving spray drying a slurry of $Al(OH)_3$ in aqueous LiOH. Product recovery was improved over earlier runs by increasing the upward velocity of the slurry from the drier nozzle. This appears to have increased the drying time for droplets in the downward flowing air, thereby reducing the number of damp particles sticking to the drier walls. The water content of the slurry feed also was reduced. In future experiments the water content will be reduced further, and the batch size will be increased.

Batches of α-$LiAlO_2$ were synthesized by calcining (at 925 K) powder obtained by spray drying a slurry prepared from Al_2O_3, Li_2CO_3, and aqueous acetic acid. The α-$LiAlO_2$ product was in the form of particle agglomerates ranging from 5 to 50 μm in size. These agglomerates, which are too large for preparing cold-pressed green bodies, are expected to break down during ball milling, which is used to prepare slips in the tape-casting process.

Tape Casting

Several attempts were made to prepare tapes suitable for sintering using α-$LiAlO_2$ powders. Serious problems were encountered with tape cracking. Discussions were held with our tape-casting consultant, Richard Mistler (Plessey Corp.), and a visit was made to his laboratories. No trial batches yet have been prepared with α-$LiAlO_2$ since that visit, but tapes have been prepared successfully with β-$LiAlO_2$.

Crack-free, pliable tapes (10 × 17 × 0.085 cm) were prepared from β-$LiAlO_2$ obtained by the spray-drying process. One tape was fired for 1 h at 1325 K, resulting in sintered γ-$LiAlO_2$ of 69% porosity. The hollow spherical agglomerates observed in the spray-dried β-$LiAlO_2$ product broke up during preparation of the slurry constituents (slip).

Stability of $LiAlO_2$ Sinters

Sintered γ-$LiAlO_2$ specimens were exposed to carbonate eutectic for 150 and 500 h at 925 K in either air or dry CO_2. In SEM examination, the particles in the 500 h samples exposed in air appear to have changed slightly toward more regular shapes. The other specimens had no apparent change.

Synthesis of $LiAlO_2$-Carbonate Eutectic Mixtures

Difficulties encountered recently in synthesizing mixtures of $LiAlO_2$ and Li_2CO_3-K_2CO_3 for use in fuel cell tiles indicated refinement of our standard procedure was required. One problem seems to have been caused by incomplete codissolution of LiOH, Li_2CO_3, and K_2CO_3 during the first heating of dry reagent powders. The problem has been eliminated by pregrinding the K_2CO_3 reagent, which was much coarser than the Li_2CO_3. A further process improvement was made by providing more effective contact of the product powders with CO_2 reactant gas so that conversion of any unreacted LiOH would be assured during the final heat treatment. The modified process results in a γ-$LiAlO_2$ powder of higher surface area than that obtained previously (36 *vs.* 20 m^2/g).

Good quality hot-pressed pellets and tiles were prepared from the products of the modified procedure. However, at a given carbonate-to-$LiAlO_2$ ratio, the tiles are stiffer with this new material, probably because of the higher surface area of the particles.

Tile Preparation

Several tiles were pressed from high-surface-area (about 30 m^2/g) γ-$LiAlO_2$ and Li_2CO_3-K_2CO_3 mixtures. A minor density variation has been observed in hot-pressed tiles and appears to have been caused by air escaping

from the die when the upper platen was inserted; this results in redistribution of some of the fine powders. The density variations have been nearly eliminated by compacting the powder prior to inserting the upper platen.

Electrode Development

Cathode Development

The lithium content has been determined for synthesized and sintered specimens of lithiated nickel oxide by precise measurements of the lattice parameters by x-ray diffraction. Samples compounded to contain 5 cation percent lithium prior to firing for one hour contain from about 4.3% when fired at 1075 K to virtually none when fired at 1575 K. Samples fired for one hour at temperatures not exceeding 1175 K have adequate lithium content for use as a fuel cell cathode.

The first cell test of a sintered and lithiated nickel-oxide cathode was conducted in this period. The results showed that the bimodal pore distribution in that cathode provides the desired (1) open pores for gas passage and (2) flooded pores for electrochemical reaction sites. However, it was found that the fraction of large pores should be larger, and the size of the agglomerates containing small pores should be smaller. Accordingly, new specimens were prepared. By using a narrow range of agglomerate sizes, greater porosity in the large pore range has been accomplished, and improved firing characteristics have been observed because of the easier escape of reaction products.

Several refinements were made in the cathode preparation. Polyvinyl alcohol, a stronger and safer binder than the stearic acid and Acryloid used previously, was employed successfully for the preparation of the cathode green body. A short precalcining of the powders prior to binder addition was shown to minimize shrinkage during the final sintering. Agglomerate size did not seem to affect product quality; this gives flexibility in optimizing pore size distribution. It was demonstrated that fines generated during preparation of the cathodes can be reused successfully.

Nickel Aluminate Preparation

In stability tests at 925 K, samples of $NiAl_2O_4$ in contact with Li_2CO_3-K_2CO_3 were maintained at 1200, 1400, 1600°C for up to about 200 h. The structures' stability was found to be a function of the particle morphology and to increase with decreasing surface area of the particles; $LiAlO_2$ appeared in nearly all samples. Surprisingly, metallic nickel appeared in many of the exposed samples.

Component Testing

Cell Testing

A cathode of preoxidized and prelithiated nickel oxide was used in cell test SQ-19. Electrochemical performance for this cell was lower than normal, probably because of a poor pore-size distribution for that cathode. Also, the tile, which had high-surface-area γ-$LiAlO_2$, was too stiff and did not conform well to the cathode's dimensional irregularities. The wet seals were established on cell heat-up and did not degrade.

An improved cathode pore-size distribution, closer dimensional control on the cathode, and a more compliant ("wetter") tile will be used for the next cathode in-cell test.

Posttest Microscopic Examination of Cell Components

The electrolyte wetting of the anode from cell SQ-19 appears to have been good. The Ni-Cr surfaces were completely covered with molten carbonates, but the pores remained open for gas passage. Although the cathode had open pores for gas passage and flooded pores for electrochemical reaction sites and ion transport, the agglomerates containing the fine pores were so large that much of the wetted surface was probably inactive.

Cell Resistance Measurement

A new current-interrupt switch was developed for use in determining cell resistance and for studying potential-relaxation characteristics of the cell. The switch gives a full on-to-off transition with a 1-A current in 50 to 100 ns.

I. INTRODUCTION

The advanced fuel cell studies at Argonne National Laboratory (ANL) are part of the DOE Advanced Fuel Cell Program. A goal of this DOE program is the earliest possible introduction of high-efficiency generating systems based on molten-carbonate fuel cells, which have the capability of operating on coal or other fuels. At the present stage of development, the primary thrust of the ANL program is to provide supporting research and development that investigates alternative stack concepts and pursues fundamental understanding of fuel cell behavior.

A molten carbonate fuel cell consists of a porous nickel anode, a porous lithiated nickel oxide cathode, an electrolyte structure which separates the anode and cathode and conducts only ionic current between them, and appropriate metal housings or, in the case of stacks of cells, intercell separator sheets. The cell housings (or separator sheets) bear upon the electrolyte structure to form a seal between the environment and the anode and cathode gas compartments. The usual electrolyte structure, which is commonly called "tile," is a composite of discrete $LiAlO_2$ particles and a mixture of alkali metal carbonates. The carbonates are liquid at the cell operating temperature of 925 K. At the anode, hydrogen and carbon monoxide in the fuel gas react with carbonate ion from the electrolyte to form water and carbon dioxide while giving up electrons to the external circuit. At the cathode, carbon dioxide and oxygen react and accept electrons from the external circuit to reform carbonate ion, which is conducted through the electrolyte to the anode. In a practical cell stack, CO_2 from the cathode probably would be obtained from anode exhaust.

The ANL contribution to the program is intended to develop improved components and processes and to provide understanding of cell behavior. Improvements are needed in the electrolyte structure and cathode, which are receiving special attention at ANL. Electrolyte structures employing a sintered $LiAlO_2$ matrix are being examined as an alternative to tiles, which are a paste-like mixture of fine $LiAlO_2$ particles and carbonate salt. Characterization of electrolyte-structure properties and the relation of the properties to cell behavior are of major importance. Determination of the stability of the structure is also of high priority.

Current practice involves assembling molten carbonate fuel cells with a sintered nickel cathode which reacts *in situ* with the oxidant gas and the electrolyte to form lithiated nickel oxide. The "lithiation" is important to give the cathode adequate electronic conductivity. ANL is investigating preparation of lithiated nickel-oxide cathodes for assembly in cells, which are expected to attain higher performance through the better conductivity, strength, and dimensional stability of the cathode.

Cells are operated to assess the behavior of the electrolyte and other components and to understand the performance and life-limiting mechanisms at work within the cell. Cell operation is coupled with efforts on diagnostics and materials development.

II. DEVELOPMENT OF ELECTROLYTE STRUCTURES

A. Preparation of $LiAlO_2$ for Sintered Structures

1. Preparation of Spray-Dried β-$LiAlO_2$ for Sintered Structures

(J. W. Sim, J. J. Slaga)

To obtain a supply of $LiAlO_2$ for tape-casting experiments, four batches of $LiAlO_2$ powder were prepared by spray drying slurries of LiOH and $Al(OH)_3$ in water. These experiments are summarized in Table 1. Three of the batches exhibited acceptable sintering behavior, but batch 207-15-600, which was mistakenly prepared with extra LiOH, sintered excessively. Product recovery was increased to 86 and 88 percent for batches 207-17-600 and 207-26-600, respectively. This improvement in product recovery was the result of an increase in atomizing pressure, from 100 to 140 kPa (~15 to 20 psi). With the pressure set at 100 kPa, the slurry droplets apparently had insufficient initial upward velocity in the downward-moving stream of hot air from the spray drier. As a result, the droplets struck the wall of the spray drier (and adhered) before they were completely dry. When the atomizing pressure was increased to 140 kPa, the droplets rose higher in the hot air stream and dried out before contacting the wall of the spray drier. Consequently, very little product buildup was observed on the wall of the spray drier, and the product recovery increased.

To increase the energy efficiency of the spray-drying process and to increase the rate of production of powder, less water was used to prepare the slurry in batch 207-26-600. The amount of water used to form a slurry of $Al(OH)_3$ powder was decreased from 1500 cm^3 to 750 cm^3, while the amount of water used to dissolve the $LiOH \cdot H_2O$ was unchanged from 1500 cm^3. The product was acceptable. It is believed that the amount of water can be decreased still further by using less water to dissolve the $LiOH \cdot H_2O$. Future experiments will be directed toward decreasing the amount of water in the slurry and increasing the batch size.

Table 1. Summary of Spray-Drying Experiments

Batch No.	Reactants	Product Recovery, %	Surface Area, m^2/g	Comments
207-14-2-600	305.0g $Al(OH)_3$ in 1500 cm^3 H_2O 162.1g $LiOH \cdot H_2O$ in 1500 cm^3 H_2O	63	26	Acceptable Sintering
207-15-600	305.0g $Al(OH)_3$ in 1500 cm^3 H_2O 164.2g $LiOH \cdot H_2O$ in 1500 cm^3 H_2O	70	--	Excessive Sintering
207-17-600	305.0g $Al(OH)_3$ in 1500 cm^3 H_2O 162.1g $LiOH \cdot H_2O$ in 1500 cm^3 H_2O	86	28	Acceptable Sintering
207-26-600	305.0g $Al(OH)_3$ in 750 cm^3 H_2O 162.1g $LiOH \cdot H_2O$ in 1500 cm^3 H_2O	88	--	Acceptable Sintering

2. Alpha-Lithium Aluminate Preparation

(J. T. Dusek, J. J. Slaga, R. M. Arons, and W. P. Leinweber)*

The large demand for powder imposed by our planned tape-casting studies, along with continued studies of composite NiO-$LiAlO_2$ plates and ongoing fabrication of sintered plates for cell tests, has necessitated the pursuit of $LiAlO_2$ production methods with higher yield rates (mass/time). We are currently investigating the applicability of spray drying a slurry of Al_2O_3 and a lithium-based solution as an alternative to the previously employed process of ball milling Al_2O_3 and Li_2CO_3 in methanol and then centrifuging and drying.

In contrast to the parallel studies being performed by Sim and Slaga (see Section II.A.1.), we are using Al_2O_3 and Li_2CO_3 as starting feedstock. These powders are then mixed into an acetic acid solution, where the reaction

$$Li_2CO_3(solid) + 2HC_2H_3O_2(solution) \rightarrow 2LiC_2H_3O_2(solution) + H_2O + CO_2(\uparrow)$$

takes place. Upon spray drying, most of the solvent and water of reaction is driven off, yielding an intimately mixed powder of Al_2O_3 and hydrated lithium acetate ($LiC_2H_3O_2 \cdot H_2O$). Our preliminary x-ray diffraction (XRD) study of the product of calcination of this material at 925 K shows it to be pure α-$LiAlO_2$.† This product is different from that obtained by spray drying a slurry of Al_2O_3 in a LiOH solution, which produces β-$LiAlO_2$ powder.

We have made 10 spray-drying runs to date using this approach. The details of these experimental runs are summarized in Table 2. Note that a small amount of Elvanol** (polyvinyl alcohol) was added to the feed. This serves as a binder and aids agglomeration of the dried spray so that the very fine powders are not lost through the collection cyclone of the spray dryer. However, the batches prepared for runs 75-15-1, 90-50-1, 75-15-2, and 90-50-2 contained insufficient acetic acid to completely dissolve the Li_2CO_3. This led to problems of gross agglomeration or clumping of the feed slurry and caused clogging of the spray dryer. Similarly, batches 75-15-5 and 75-15-15A, which had no acetic aid, were very thixotropic and would not flow. Addition of 300 cm^3 of water allowed proper flow.

This process produces moderately sized agglomerates (>5 μm, <50 μm), which are unsuitable for cold pressing directly onto flat structures for sintering. We expect, however, that the agglomerates will be broken down during ball milling of tape-casting slips.

B. Tape Casting

Tape casting is under development as a method of fabricating green bodies that can be fired to produce porous plates of sintered $LiAlO_2$. This method is being investigated because, unlike other ceramic fabrication techniques,

---

*Materials Science Division, ANL.

†X-ray diffraction performed by B. S. Tani, Analytical Chemistry Laboratory, ANL.

**Trade name of DuPont.

Table 2. Summary of α-$LiAlO_2$ Spray-Drying Experiments

Run No.	Al_2O_3, g	Li_2CO_3, g	Elvanol 75-15, g	Elvanol 90-50, g	Acetic Acid, cm^3	H_2O, cm^3	Inlet Temp., °C	Outlet Temp., °C	Air Pressure, psi	Comments
75-15-1	111.00	73.89	1.85	-	62	1940	315-320	120-125	15	Flow problems due to undissolved Li_2CO_3.
90-50-1	↓	↓	-	1.85	65	1875	315-320	120-125	↓	
75-15-2			1.85	-	70	1850	310-315	110-120		
90-50-2			-	1.85	-	1550	310-315	110-120		
00-1			-	-	155	1175	310-315	110-115		Good spray-drying properties.
75-15-3			1.85	-	155	1175	225	88-90		
75-15-4	333.00	221.67	5.55	-	465	3525	220-228	88-90	14	
75-15-4A	333.00	221.67	5.55	-	465	3525	220-228	88-90	14	
75-15-5	111.00	73.89	1.85	-	-	1500	220-230	96-100	15	Thixotropic nature of slurry required addition of extra 300 cc H_2O to create proper flow properties.
75-15-5A	111.00	73.89	1.85	-	-	1500	220-230	96-100	15	

it produces a thin green body that possesses considerable handling strength. The tape-casting process involves several steps. In the first step, slip formulation, the $LiAlO_2$ powder is dispersed in a solution containing a polymeric binder. Plasticizers are sometimes included in the slip formulation to improve the flexibility of the green body (dried tape). A deflocculant is also used to aid in dispersing the powder and to stabilize the resulting dispersion. When the slip formulation is complete, air is removed from the dispersion by reducing the pressure in a chamber containing the slip. In the second step, casting, the slip is leveled to a controlled thickness by moving a doctor blade at a controlled height across a pool of the slip on a casting surface. In actual production, the casting surface would be moved, while the doctor blade would remain stationary. In the final step of the tape-casting process (drying), the solvents in the cast slip are evaporated, leaving a flexible sheet in which the $LiAlO_2$ particles are held together by the polymeric binder.

1. Tape Casting of α-$LiAlO_2$

(J. T. Dusek, R. M. Arons)*

A series of 13 trial runs was made to determine how well $LiAlO_2$ mixes with the various materials suggested for use in tape casting by our consultant, Richard Mistler (Plessey Corporation). The results were forwarded to Mistler along with several photographs showing tape-casting results. The tape-cast batches were covered during drying to slow the drying process, but all showed severe cracking in overnight drying. Because our $LiAlO_2$ is of such high surface area (~50 m^2/s), large volumes of solvent compared to conventional Al_2O_3 tape casting have been required. This enhances shrinkage on drying, which may be the cause of the cracking.

Three additional trial batches were prepared after consultation with Mistler. In these, cracking was delayed but not prevented.

On November 17, 1980, three ANL staff--R. M. Arons, J. T. Dusek, and J. Sim--visited Plessey Corp. in Frenchtown, NJ, to observe the tape casting of an experimental slip and to discuss our problems with Mistler. No additional trial batches have been prepared with α-$LiAlO_2$ since that visit, but experiments with spray-dried β-$LiAlO_2$ are reported below.

2. Tape Casting of Spray-Dried β-$LiAlO_2$

(J. W. Sim)

During this quarter, tape-casting experiments using spray-dried β-$LiAlO_2$ powder in the slip formulation were initiated. These preliminary experiments provided considerable information on the conditions required to produce a useful green body via tape casting. A crack-free tape was cast with the approximate dimensions of 10 by 17 by 0.85 cm. The tape was flexible and had considerable handling strength. A sintered structure of about 69 percent porosity was produced when a portion of one of the tapes was heated at 1325 K for about 1 h. This result demonstrates that a sintered $LiAlO_2$ structure of the desired porosity (≥60 percent) can be fabricated by tape casting the green body. Microscopic examination (SEM) of the

*Materials Science Division, ANL.

sintered structure indicated that the hollow spherical agglomerates in the spray-dried $LiAlO_2$ powder had broken down during ball milling of the slip. In the past, when pellets were pressed and sintered from spray-dried $LiAlO_2$ powder, the spherical agglomerates remained intact, resulting in some large (about 1-10 μm) pores. Tape casting, therefore, eliminates some of the larger pores produced when spray-dried $LiAlO_2$ is used to prepare sintered structures.

The slip formulations in which spray-dried $LiAlO_2$ was used are given in Table 3, and the tape-casting experiments are summarized in Table 4. Information on the constituents in the slip is presented in Table 5. All of the cast slips were dried slowly by placing them in a small cabinet that was purged with a low flow of nitrogen; complete drying occurred sometime between five and twenty hours. Although such slow drying probably is unrealistic for production of large quantities of tape, we used this drying procedure to minimize problems that might occur if the solvent is driven off too quickly (e.g., bubble formation). In future experiments we will examine faster drying schedules.

Table 3. Slip Formulations Using Spray-Dried β-$LiAlO_2$

	Weight, g	
	SN-207-20	SN-207-25
$LiAlO_2$[a]	87.3	63.8
Solvent	202[b]	102[c]
Deflocculent	1.8	3.8
Plasticizer		
PX316[d]	3.6	8.5
UCON[e]	4.9	11.5
Binder	7.0	13.6

[a]Sample number 207-17-600, 28 m^2/g.

[b]28 wt % ethanol and 72 wt % trichloroethylene.

[c]40 wt % ethanol and 60 wt % xylene.

[d]Mixed normal alkyl phthalates, USS Chemicals.

[e]Polyethylene glycol, Union Carbide product UCON-50-HB-2000.

Table 4. Tape-Casting Experiments on Slip Formulations from Table 3

Tape No.	Slip No.	Casting Surface	Blade Opening, cm	Comments
T-207-22-1	SN-207-20	ACLAR[a]	0.165	Skin formed during casting. Cracked into pieces of about 10 cm^2. Easy release of dried tape from casting surface. Sintered to 69% porosity.
T-207-22-2	SN-207-20	Cellulose Acetate	0.165	Cellulose acetate did not lie flat during casting and warped during drying of tape. Dried tape adhered to cellulose acetate.
T-207-27-1	SN-207-20	ACLAR	0.165	Cracked into pieces about 4 cm^2. Easy release of dried tape from casting surface.
T-207-27-2	SN-207-20	Graphite-coated ACLAR	0.127	Cracked into pieces about 4 cm^2. Dried tape adhered to casting surface.
T-207-27-3	SN-207-25	ACLAR	0.165	Cracked into three pieces ranging in size from about 10 cm^2 to about 75 cm^2. Easy release of dried tape from casting surface. Pieces of tape were very flexible.
T-207-27-4	SN-207-25	Graphite-coated ACLAR	0.165	Multiple cracks occurred. Dried tape adhered to casting surface. Pieces of tape were very flexible.
T-207-29	SN-207-25	Teflon-coated glass	0.165	Crack-free tape, about 10 x 17 x 0.085 cm. Easy release of dried tape from casting surface. Dried tape was very flexible.
T-207-31	SN-207-25[b]	Uncoated glass	0.165	Three cracks in dried tape. Pieces ranged in size from about 10 cm^2 to about 70 cm^2. Tape was destroyed because of adherence to glass surface. Air bubbles observed in cast slip.
T-207-32	SN-207-25	Teflon-coated glass	0.165	Multiple cracks in dried tape. Multiple air bubbles in cast slip. Easy release of dried tape from casting surface. Dried tape was flexible.

[a] A fluorohalocarbon film produced by Allied Chemical.

[b] Slip was not de-aired prior to casting.

Table 5. Constituents of Slip Formulation

Constituent	Manufacturer	Function	Chemical Description	Density, g/cm^3	Boiling Point, °C
$LiAlO_2$ powder	--	--	Spray-dried β-$LiAlO_2$	2.6	—
Ethanol	--	Solvent	—	0.79	78.5
Trichloro-ethylene	—	Solvent	—	1.46	87
Xylene	—	Solvent	Mixed xylene isomers	0.86-0.88	138-144
Kellox Z-3 fish oil	Spencer Kellogg	Deflocculant	Mixed unsaturated fatty acid esters of glycerol	0.98	—
PX 316	USS Chemicals	Plasticizer	Mixed normal alkyl phthalates	0.97	250 at 5 mm Hg
UCON 50-HB 2000	Union Carbide	Plasticizer	Polyalkylene glycol	1.06	—
Butvar B-98	Monsanto	Binder	Polyvinyl butyral	1.10	—

Based on the limited number of experiments summarized in Tables 3 and 4, we have drawn the following conclusions:

1. The surface onto which the slip is cast must be level and free from ripples.

2. The dried tape does not adhere to teflon-coated glass or ACLAR (a fluorohalocarbon film produced by Allied Chemical) surfaces, but it does adhere to uncoated glass, cellulose acetate, and graphite-coated ACLAR surfaces. Adhesion of the dried tape to the casting surface can prevent removal of intact tapes from the surface.

3. The use of xylene in place of trichloroethylene as a solvent greatly reduced "skin" formation on the surface of the slip during casting. The "skin" forms as solvent evaporates, and xylene is less volatile than trichloroethylene.

4. Air entrapment in the cast slip probably contributes to cracking of the tape. Air may become entrapped when pouring the slip onto the casting surface and/or during leveling. Also, if the vacuum de-airing of the slip is not complete, air entrapped during ball milling of the slip may be present.

We believe that, in obtaining an acceptable tape, the casting variables (i.e., composition and condition of the casting surface, rate of movement of the doctor blade, magnitude of the doctor blade opening, and the drying rate) are at least as important as the slip formulation variables (i.e., relative amounts of the $LiAlO_2$ powder, solvent, binder, plasticizer and deflocculant). Consequently, casting variables will be controlled carefully in future experiments. In particular, we plan to mechanize the movement of the doctor blade in order to achieve better control of the rate of movement of the blade. Slip formulation variables will continue to be investigated as well.

C. Stability of $LiAlO_2$ Sinters

(G. H. Kucera)

Studies to assess the effects of time and gaseous environment on the microstructure of γ-$LiAlO_2$ sinters impregnated with Li_2CO_3-K_2CO_3 eutectic are continuing. The initial sintered γ-$LiAlO_2$ structures were prepared by heating cold-pressed (one-inch diameter) discs of spray-dried β-$LiAlO_2$ that had been sintered at about 1275 K in air for about 1 h. The porosities of these structures ranged between 62.6 and 65.2 percent. The tests were conducted on specimens that contained an average of 64.2 vol % carbonates and were exposed to either an air or dry CO_2 environment at 925 K. Samples were taken at about 150 and 500 h. The fracture surfaces of portions of the sinters, washed free of carbonates, were examined by scanning electron microscopy (SEM).

The SEM examination was made on portions of three sinters held at 925 K, one in dry CO_2 for 168 h and two in air for 144 and 503 h. Baseline characteristics were established by SEM examination of fracture surfaces of an unimpregnated sinter and a carbonate-impregnated sinter that had not been

subjected to further heat treatment. The SEM micrographs showed that both baseline sinters consisted of agglomerates in which the individual particles were <0.5 μm. The SEM data on the test sinters suggest that little or no particle growth occurred in either the air or dry CO_2 environment in the time intervals studied to date. However, the shape of the particles in the specimen exposed to an air environment for 503 h became more defined; they were best described as regular polyhedra. Porosimetry measurements will be made to determine the accompanying effect on pore size.

D. Synthesis of $LiAlO_2$-Carbonate Eutectic Mixtures

(G. H. Kucera)

Difficulties encountered recently in the synthesis of mixtures of $LiAlO_2$ and Li_2CO_3-K_2CO_3 eutectic for use in fuel cell tiles indicated that a modification of the standard ANL method for producing the mixtures[1] was required to improve the reliability of the process and the quality of the product. The difficulties included varying degrees of product caking, the presence of a low-melting (about 635 K) salt, and variations in the $LiAlO_2$ powder characteristics. During this quarter, in support of cell testing efforts, we modified the synthesis procedure and tested the quality of the product; the quantities and kinds of reactants, i.e., Degussa γ-Al_2O_3, LiOH, Li_2CO_3, and K_2CO_3, were not changed.

The previously published procedure[1] used a two-step heat treatment; the first at 775 K in an air environment produced a reaction between LiOH and γ-Al_2O_3 to form $LiAlO_2$, and the second at 975 K in a dry CO_2 environment converted any unreacted LiOH to Li_2CO_3 and assured complete reaction of the γ-Al_2O_3. We now believe that, with the fine powder Li_2CO_3 and coarser granular K_2CO_3 that were used, (1) little or no 62 mol % Li_2CO_3-38 mol % K_2CO_3 eutectic (mp, 766 K) was formed after the 775 K treatment and (2) some, but not all, Li_2CO_3 (mp, 996 K) and K_2CO_3 (1171 K) combined to form the eutectic even after the 975-K treatment. The procedure has been modified to include the use of ground (<250 μm) K_2CO_3. In samples prepared by this modified procedure (Fig. 1), evidence of eutectic formation was seen in the lightly caked, agglomerated product of the 775-K treatment and the highly caked product of the 925-K treatment. The final product was ground to a free-flowing powder with moderate effort.

Evidence of a low-melting salt in the $LiAlO_2$-carbonate mixture produced by the standard method was noted by Smith and Stapay, ANL, during the hot pressing of an electrolyte tile. A portion of the electrolyte powder melted and extruded from the die at a temperature below the melting point of the carbonate eutectic. Subsequent thermograms (heating and cooling curves) were obtained from differential thermal analysis (DTA) on portions of the $LiAlO_2$-eutectic mixture. These curves showed the presence of a low-melting salt (about 633 K) as well as the expected Li_2CO_3-K_2CO_3 with a slightly off-eutectic composition. The literature[2] cites two ternary eutectics in the LiOH-Li_2CO_3-K_2CO_3 system with melting points at 645 and 623 K. This suggests that the conversion of LiOH (mp, 750 K)[2] to Li_2CO_3 in the second step (975 K in CO_2) was incomplete.

Fig. 1. Revised Method for Preparing $LiAlO_2$-Electrolyte Mixtures Containing a Major Phase of γ-$LiAlO_2$

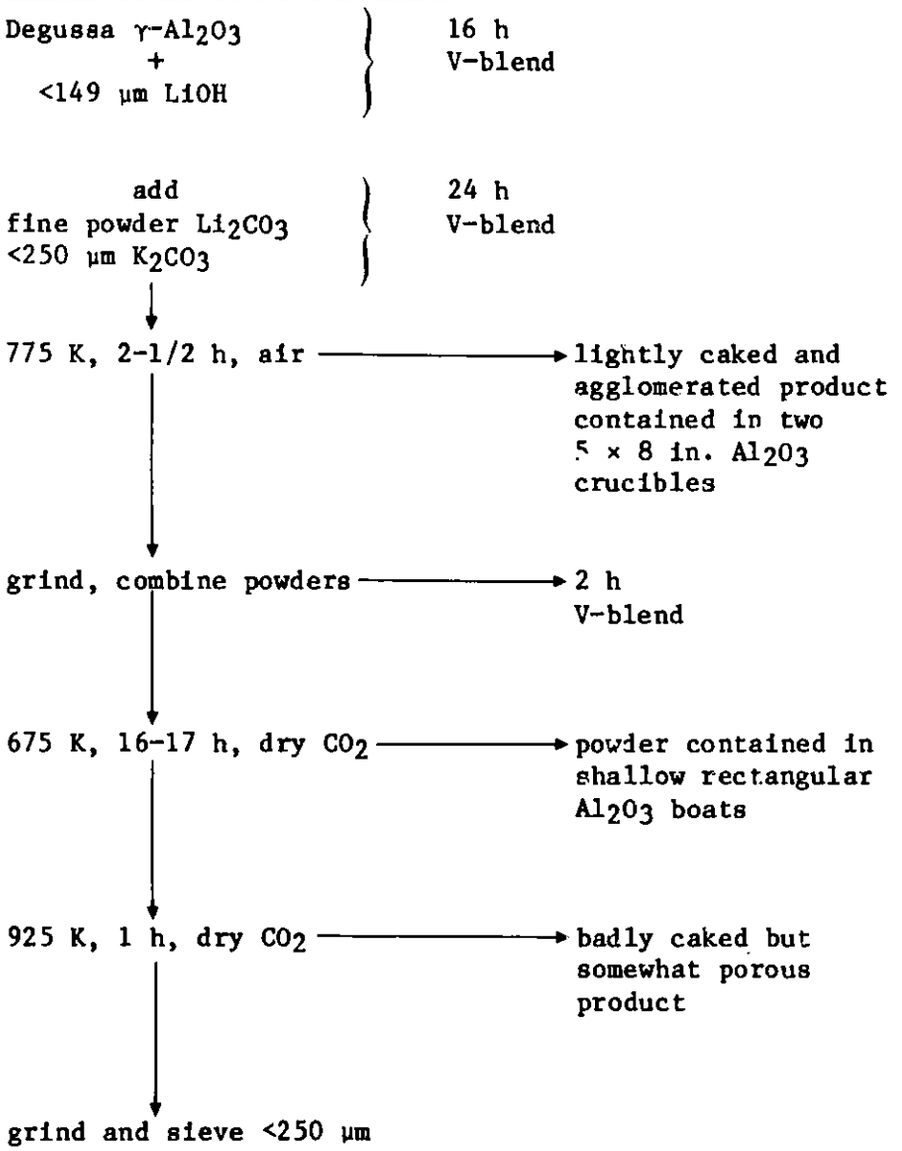

In the modified procedure, to assure complete LiOH-to-Li_2CO_3 conversion, the powder is spread in thin layers ($\leq$6 mm) on high-purity, high-density Al_2O_3 trays and heated in a dry CO_2 environment to 673 K and held at that temperature for 16 h; DTA thermograms confirm that this treatment results in complete LiOH-to-Li_2CO_3 conversion.

Two 530 g batches (no. 18-68 and 18-74) of high-surface-area $LiAlO_2$ and 62.5 wt % Li_2CO_3-K_2CO_3 eutectic were produced by the modified procedure. Physical characterization of the $LiAlO_2$ powder in batch no. 18-68, which

was undertaken with x-ray diffraction analyses* and BET surface area measurements,† indicated γ-$LiAlO_2$ as a major phase and β-$LiAlO_2$ as a minor phase and a surface area of 36 m^2/g. Two electrolyte tiles were pressed from batch no. 18-68; one was used in test cell SQ-19 (see Section IV). The $LiAlO_2$ in batch no. 18-74, which was characterized only by x-ray diffraction analysis, contained γ-$LiAlO_2$ as a major phase and β-$LiAlO_2$ as a medium phase.

The data obtained from cell SQ-19 suggested that the electrolyte tile pressed from batch no. 18-68 was too stiff to deform adequately, thereby not compensating for dimensional irregularities of the cell components; consequently, the electrolyte content in a portion of batch no. 18-74 was increased from 62.5 to 64.0 wt % (70.4 vol %). This was achieved by adding the required amount of electrolyte in the form of premelted, ground eutectic and heating the mixture to about 825 K in dry CO_2 for about 0.5 h. The physical characterization of the $LiAlO_2$ from this portion, now labeled batch no. 18-76, by BET surface area and x-ray diffraction measurements, showed that the powder had a surface area of 30 m^2/g and still contained γ- and β-$LiAlO_2$ as major and medium phases, respectively.

The thermomechanical behavior of a small (1.25-cm dia) hot-pressed pellet fabricated with powder from batch no. 18-76 was monitored in a dilatometer from room temperature to about 785 K under a stress of 41.5 kPa. The data at 785 K show that a 50% compression of the pellet was achieved in about five minutes. This test showed that the material was promising for use as an electrolyte tile, because component wetting in a cell would occur in coincidence with tile compliance. A tile has been pressed from batch no. 18-76 for use in a future test cell.

In summary, the electrolyte mixtures produced, thus far, by the revised method appear attractive for use in test cells and capable of supporting electrolyte contents >70 vol %. However, more data are required to verify the reproducibility of this method.

E. Tile Preparation

(J. L. Smith and J. R. Stapay)

Several tiles have been pressed from powders containing high-surface-area (about 30 m^2/g) lithium aluminate and Li_2CO_3-K_2CO_3 eutectic. Cell SQ-19 used a tile of this material with 62.5 wt % carbonates. Similar tiles have been made with 64 wt % eutectic.

A minor but persistent density variation in our tiles has been observed by x-ray radiography. It appears that this was caused by air escaping from the die when the upper platen was inserted, thereby redistributing tile material. The density variation has been nearly eliminated by compacting the powder in the die prior to installing the upper platen.

---

*Performed by B. S. Tani, Analytical Chemistry Laboratory, ANL.

†Performed by R. Malewicki, Analytical Chemistry Laboratory, ANL.

III. ELECTRODE DEVELOPMENT

A. Cathode Development

(R. M. Arons, J. T. Dusek, and J. J. Slaga)*

Although most of the lithiated NiO specimens used in our studies reported previously were compounded to contain five cation percent lithium, volatilization of Li_2CO_3 and Li_2O during the firing led to a lower lithium content in the sintered NiO. Assessment of the final lithium content is difficult because conventional electron probe techniques do not detect low atomic number elements such as lithium. Further, other techniques such as wet chemistry do not assess how much lithium is actually in the lattice.

Another technique, which has been favored by investigators at Oak Ridge National Laboratory (ORNL),[3] is to exploit the subtle lattice parameter shift in NiO, which takes place as Li^+, a smaller cation than Ni^{2+}, is dissolved into the lattice. Using the study of Toussaint[4] as a calibration, one can correlate lithium content with precisely measured lattice parameters from x-ray diffraction (XRD).

Following such a procedure, XRD was performed† on six specimens (numbered 16-1 through 16-6) reported on previously (ANL-81-16, p. 22). Table 6 gives the lattice parameter data and the correlated cation percent Li^+ along with previously reported density and resistivity data. Figure 2 shows the variation of lithium content with sintering temperature plotted using the data in Table 6. Given that the equilibrium concentration of lithium in an operating molten carbonate fuel cell is roughly 2.5 cation %,[4] any 1-h firing of $Li_{0.05}Ni_{0.95}O$ at 1050°C or less appears to produce both adequate final lithium content (which minimizes "break-in period" and electrolyte lithium loss) and electrical conductivity.

Table 6. Data on Lithiated NiO after Sintering for 1 h (originally compounded with 5 cation % Li^+)

Specimen Number	Sintering Temp., °C	Density, g/cm^3	Resistivity, ohm·cm	Lattice Parameter, A	Cation Percent Li+
16-6	800	2.997	3.65	4.169	4.38
16-1	900	3.382	2.80	4.171	3.25
16-2	1000	3.907	2.35	4.172	2.69
16-3	1100	4.319	2.34	4.172	2.69
16-4	1200	4.376	4.58	4.1737	1.735
16-5	1300	5.338	22.9	4.177	0

*Materials Science Division, ANL.

†X-ray diffraction performed by B. S. Tani, Analytical Chemistry Laboratory, ANL.

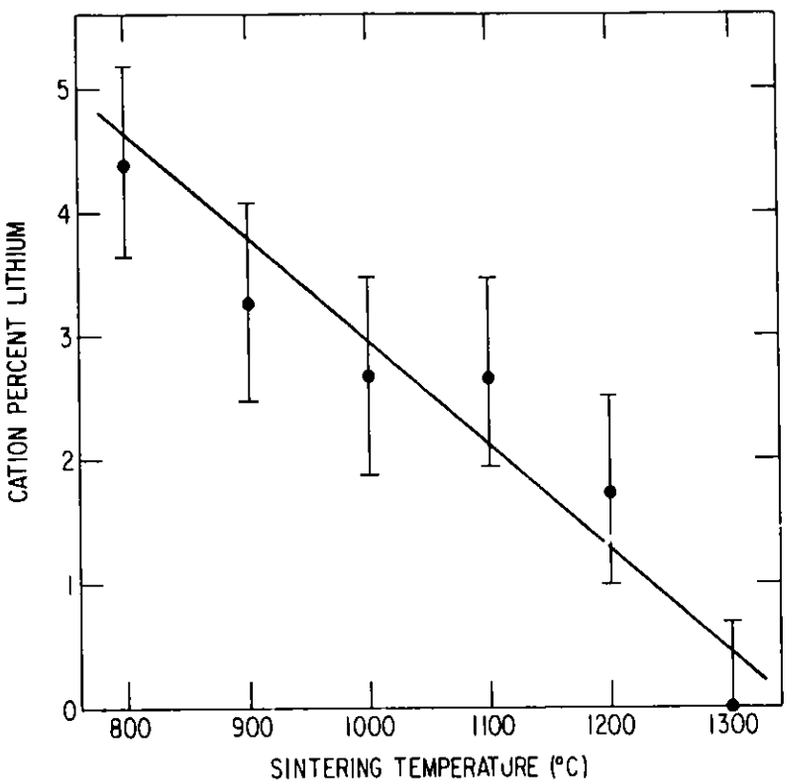

Fig. 2. Variation of Residual Lithium Content in NiO with Firing Temperature for 1-h Soak as Measured by XRD Lattice Parameter Shift Technique. Original lithium content was 5 cation %.

The standard preparation of lithiated NiO as described in ANL-80-98, pp. 11-15, utilizes an unsintered agglomerate size of -200 mesh, i.e., all agglomerates were -200 mesh or smaller. A cathode fabricated by such a technique was used in cell test SQ-19 (see Section IV). Cell performance and posttest microscopy indicated that, in this cathode, the coarse porosity (between agglomerates) was not extensive enough and that much of the flooded fine porosity (within agglomerates) was too far from the gas-liquid interface to provide active electrochemical sites. It was concluded that the use of -200 mesh agglomerates does not bring about the large open pore structure desired. The wide gradation of agglomerate sizes allowed some smaller agglomerates to fill the interstices between the larger agglomerates. As a result, the coarse porosity was filled by smaller particles, and the desired pore-size distribution was lost. A second drawback to this pore filling was the occasional formation of minor blistering upon firing of the cathode. We believe that this is due to the lack of paths for decomposing binder to egress from the sample when pore channels are clogged with small agglomerates.

A series of new experiments was initiated in which two new size fractions of agglomerates (-200 +325 and -325 mesh) were used to fabricate plates of test-cell size (about 10-cm square). The -200 +325 mesh size was chosen to

obtain a narrower spectrum of agglomerate sizes so that the filling of large pores with small agglomerates could be prevented. The -325 mesh was used as a control experiment to observe effects of agglomerate size.

The -200 +325 plates fired nicely and did not blister. The shrinkage on firing was less than that of the original -200 type plates, 14.6% shrinkage for plate PC#9 with the -200 +325 mesh agglomerates versus 20.0% for PC#4 with the -200 mesh agglomerates. Final porosities were 54.9% and 41.8%, respectively. Without further substantiation, it would appear that the -200 +325 mesh material should have less loss of coarse porosity, as desired. Plates sintered from the -325 mesh agglomerates developed large, bloated blisters and irregular shrinkage, thereby indicating that the fine agglomerates impede gas release and promote pore-closing shrinkage.

Another factor that contributes to the loss of coarse pore volume is the breakdown of agglomerates during either the pressing operation or binder burnout. Agglomerate breakdown during pressing is localized mostly at the as-pressed surface due to locally high stresses at the contact points. The resistance to such agglomerate crushing is essentially a function of the strength of the polymerically bound agglomerates of the green body. Crushing of agglomerates along the free surface is undesirable because it could create a barrier to gas passage. Avoidance of such an effect is therefore important.

In an effort to minimize agglomerate breakdown and to further improve the coarse pore structure, a new series of experiments was undertaken. Four variables were investigated to determine their ultimate effects on the fired bodies. These variables are

1) binder type: stearic acid and Acryloid (SA) vs. polyvinyl alcohol (PVA),

2) binder weight fraction,

3) additions of precalcined vs. virgin powders,

4) agglomerate size range: -200 +270 mesh, -270 +325 mesh, and -200 +325 mesh.

A summary of experimental conditions is given in Table 7.

Binder Type and Weight Fraction. In comparison with SA, PVA is a stronger binder and can be used in lesser amounts. Moreover, it is water soluble (as opposed to use of carbon tetrachloride solvent for the SA system), providing easier and safer handling, and insoluble in some conventional tape-casting vehicles, such that the bonded agglomerate may be preserved during a possible tape-casting operation. Comparison of specimens 23-1 and 23-2 with 20-7 and 20-8 shows that PVA and SA specimens yield virtually identical agglomerate retention during firing (see Fig. 3). In addition, PVA specimens result in less shrinkage upon firing and a lower final density. After comparing specimens 24-1 and 24-2 with 23-1 and 23-2, we concluded that 2-1/2% PVA is insufficient to preclude crushing of agglomerates (see, for example, Fig. 4) during pressing or dusting of some powder from the agglomerates.

Table 7. Summary of Recent Lithiated NiO Sintering Experiments (NiO compounded with 5 cation % Li^+)

Specimen #	Agglomerate Mesh Size	Precalcination Conditions	Binder Type and Quantity	Firing Conditions	Density, g/cm^3	% Shrinkage on Firing	Comments
20-7	-200 +270	Virgin	16% SA[a]	1000°C, 1 h	3.169	13.8	Good pore structure with some agglomerate forming.
20-8	-270 +325	Virgin	16% SA	1000°C, 1 h	3.493	15.7	Good pore structure with some agglomerate forming.
22-1	-200 +270	1000°C, 1 h	5% PVA[b]	1000°C, 1 h	2.798	2.2	Good pore structure--excellent agglomerate retention.
22-3	-270 +325	1000°C, 1 h	5% PVA	1000°C, 1 h	2.766	1.9	Good pore structure--excellent agglomerate retention.
23-1	-200 +270	Virgin	5% PVA	1000°C	2.956	10.9	Marginally less pore retention than 22-1.
23-2	-270 +325	Virgin	5% PVA	1000°C	3.011	11.1	Marginally less pore retention than 22-1.
24-1	-200 +270	Virgin	2-1/2% PVA	1000°C	3.443	11.4	Similar to 23-1, with some additional dusting.
24-2	-270 +325	Virgin	2-1/2% PVA	1000°C	3.606	11.8	Agglomerate collapse at pressed surface.
19-7	-200 +325	1000°C, 6 h	16% SA	1000°C	2.941	8.2	Extensive agglomerate collapse throughout.
23-3R[c]	-200 +270	Virgin	5% PVA	1000°C	3.346	11.7	Not characterized.
23-4R	-270 +325	Virgin	5% PVA	1000°C	3.359	12.1	Not characterized.

[a]SA denotes 33% stearic acid with 67% Acryloid.

[b]PVA denotes 100% polyvinyl alcohol.

[c]R denotes recycled green-body material.

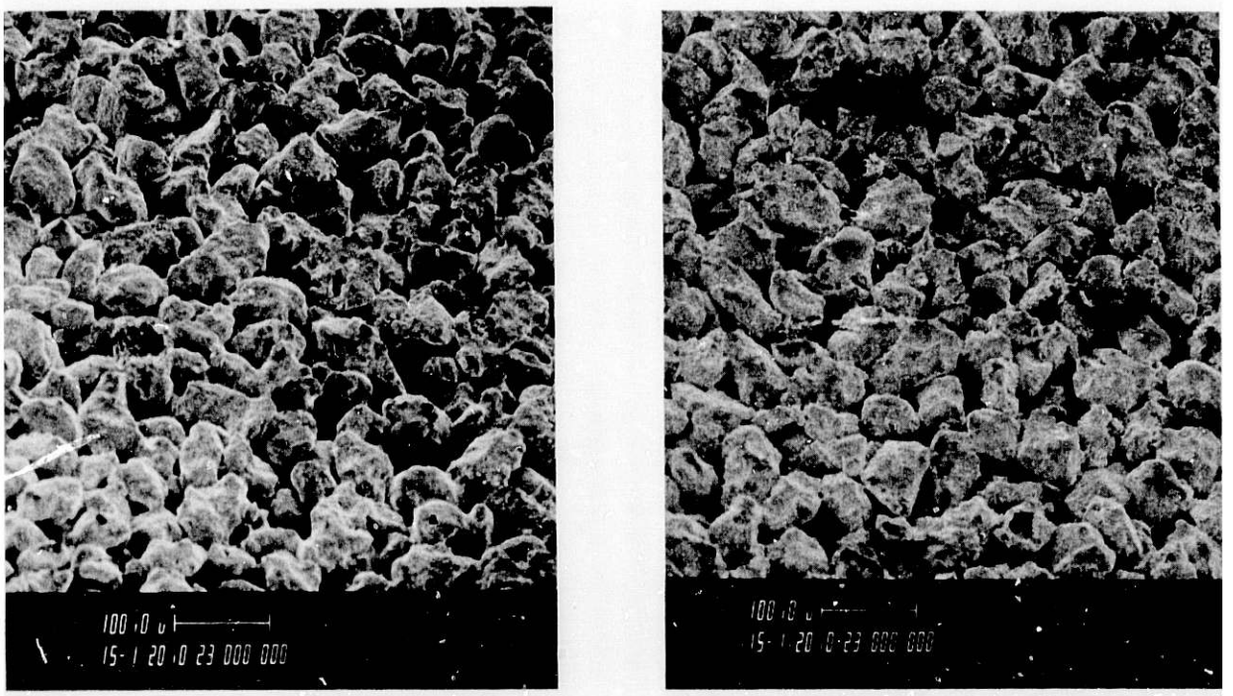

(a) Specimen 20-7 with SA (150X)

(b) Specimen 23-1 with PVA (150X)

Fig. 3. Micrographs of Fired NiO Showing Equivalent Structure Obtained via both SA and PVA Binder Systems (ANL Neg. No. 308-81-191)

Precalcination. A common approach to minimization of sintering shrinkage in ceramics is "deactivation" of the powder by precalcining it to lower surface area. Precalcination of 1 h at 1000°C prior to binder addition and crushing operations (specimens 22-1, 22-3) resulted in the least firing shrinkage (1.9-2.2%), the lowest sintered density (2.77-2.80 g/cm^3), and the best retention of coarse porosity of any specimen fired to data. Figure 5 shows the bimodal pore structure and the agglomerate shape retention on one of these specimens. If, on the other hand, one increases the precalcination time to 6 h (specimen 19-7), the structure almost completely collapses on binder burnout, as shown in Fig. 6. Although unconfirmed at present, this effect is probably due to the fraction of binder being too high to bond the particles, which have substantially lower surface area resulting from the calcination. Such a condition would produce thicker liquid layers at the particle surfaces during binder melting, allowing slumping to take place.

Agglomerate Size. The choice of agglomerate size range appeared to have little effect on the ultimate quality of the fired product. It appears that if all other variables are optimized, one may select whatever mesh size (within reason) will result in the desired final pore distribution.

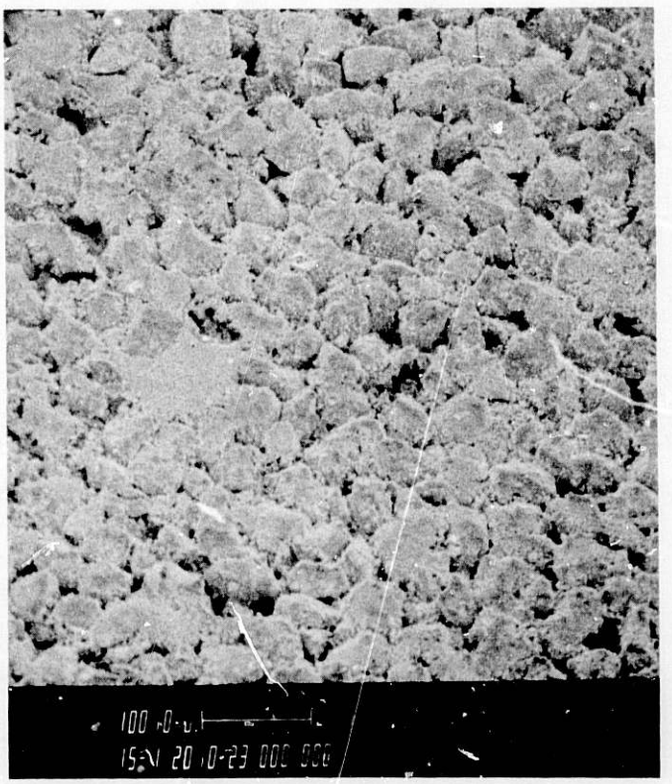

(150X)

Fig. 4. Micrograph of Specimen 24-2 Showing Extensive Crushing of Agglomerates at the Pressed Surface (ANL Neg. No. 308-81-192)

The selective use of specific agglomerate sizes results in a substantial fraction of fine agglomerates (about 14%) lower than 325 mesh. Economical use of raw material would dictate that these fines be recycled if possible. Since the agglomerates are bonded only by a soluble polymer, it is a simple matter to redissolve the binder, evaporate the new solvent, and recrush the material. This was done with specimens 23-3R and 23-4R to demonstrate feasibility of recycling. These recycled specimens showed very similar densities after firing and no apparent inferior qualities to specimens 23-1 and 23-2.

B. Nickel Aluminate
(A. V. Fraioli)

In a previous report (ANL-81-16, p. 24) techniques for preparing a variety of nickel aluminates from commercial substrate aluminas were described. Recapitulating, two calcine aluminas (C-5R, C-70) and one hydrated alumina (Catapal "SB") were separately mixed with stoichiometric quantities of $Ni(NO_3)_2 \cdot 6H_2O$, heated to 250°C for 2 h to decompose the nitrate to NiO, and then infused for additional 2-h periods at 1000°C to form $NiAl_2O_4$.

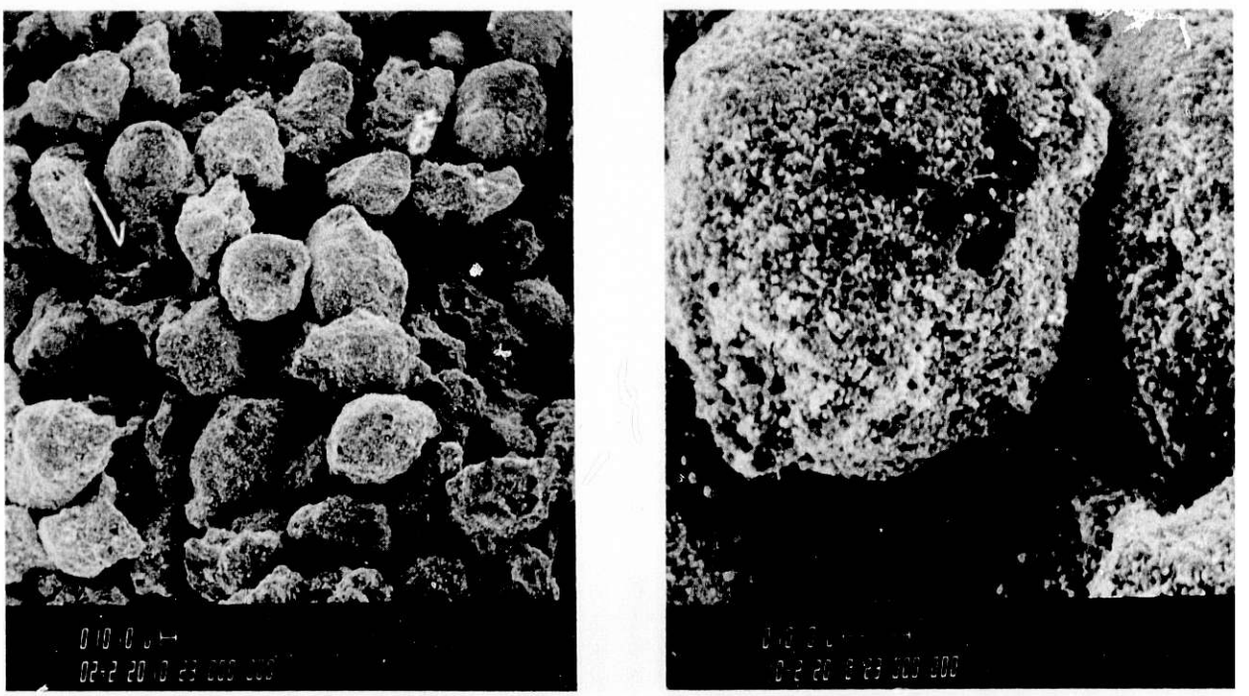

(200X) (1000X)

Fig. 5. Micrographs of Specimen 22-1 Fabricated from Precalcined Material with PVA Binder (ANL Neg. No. 308-81-193)

Subsequently, aliquots were refired an additional two hours at 1200, 1400, or 1600°C and then acid-washed to remove unincorporated NiO. In this report period, stability testing was conducted on nine of these aluminates and their three precursor substances in molten Li_2CO_3-K_2CO_3 eutectic mixtures.

The initial surface area determinations of the substrate aluminas prior to molten carbonate immersion are shown in Table 8.* Samples with areas above 10 m^2/g were measured by BET nitrogen adsorption, while those below this level were measured with krypton as adsorbate. Duplicate and triplicate measurements of the krypton-derived data show surprisingly good precision, even when obtained by two operators with the same equipment (Micromeritics Surface Area Analyzer). In accordance with the procedure established by Lessing et al.,[5] a short-term (about 200 h) aging of the nine aluminate and three precursor alumina samples was initiated. Samples consisting of 0.1 g of ceramic powder and 0.2 g premelted, ground eutectic electrolyte were placed in gold foil cups and heated in an 80% H_2-20% CO_2 atmosphere which is humidified. The atmosphere, which is employed in this Laboratory

*B. Tani and R. Malewicki of the Analytical Chemistry Laboratory conducted XRD and BET measurements, respectively.

(200X)

Fig. 6. Micrograph of Specimen 19-7 Showing Extensive Collapse of Agglomerates upon Binder Melting (ANL Neg. No. 308-81-194)

Table 8. Surface Areas of Sintered Nickel Aluminates

Precursor Alumina	Precursor Area, m^2/g	Sinter Area, m^2/g			
		1000°C	1200°C	1400°C	1600°C
C-5R Ground	2.0	1.5	1.15 ± 0.010	0.74 ± 0.02	0.61 ± 0.05[a]
C-70	32	20.5	8.44 ± 0.04	3.23 ± 0.06	0.94 ± 0.02
Catapal SB	303 ± 15	60.7	1.09 ± 0.07	0.693 ± 0.009[a]	0.241 ± 0.003[a]

[a]Designates average deviation of three separate determinations; other data are for one or two determinations.

as a fuel in cell testing, was confined in a novel quartz bell jar that had been liquid-gallium ring-sealed to a quartz base plate; this bell jar had previously shown seal integrity for 48 h under the above operating conditions. Twelve samples were withdrawn after 25 h exposure, and twelve more after 99 h sampling period. It was noted that a porous semi-solid mass (gallium/gallium silicate) had formed during the 25-99 h time interval, indicating loss of seal integrity. Another set of twelve samples was then aged in air at 650°C for the balance of the test and withdrawn after a total of 192 h.

The results of XRD analyses for the twelve-sample sets at the four aging intervals (t=0 for nonwetted sample) are shown in Fig. 7. The first three of the twelve-sample sets are for the precursor aluminas, which initially (t=0) showed α, α plus γ, and γ phases, respectively. On aging in molten eutectic, the three phases of $LiAlO_2$ were formed by the calcined aluminas (C-5R, C-70), while the hydrated alumina (Catapal "SB") showed the α and β phases but not the γ phase up to 200 h.

Examination of the data for the fired nickel aluminate substantiates Lessing's conclusion[5] that increased chemical stability may be found in other than $LiAlO_2$ compositions "if in a dense monolithic form." Unreacted alumina was not detected in aluminates formed at 1400 and 1600°C sintering temperatures (t=0), but was discovered in all three 1200°C sinters. On aging in the molten carbonate, >50% of the $NiAl_2O_4$ phase was retained in the 1600°C sinters; the decay in the peak value at the last time interval (t=192 h) was inversely related to the original surface areas of the $NiAl_2O_4$ sinters (0.61, 0.94, and 0.24 m^2/g, respectively). The resistance to formation of reaction products with the melt decreased with decreasing sintering temperature and, more specifically, was inversely proportional to the surface area of the particles prior to wetting (see Table 8).

With the 1600°C sinters, the nickel aluminates formed more completely. Thus, the appearance of new-phase material on aging may be examined more critically than with samples sintered at lower temperature. Note the gradual decrease in NiO concentration in the first stages of aging for the "SB" sample, followed by an abrupt rise in the last samples taken. If the decrease in NiO over the first two time intervals is due to the initial reducing atmosphere, why is there no concomitant rise in metallic nickel in that period? A further anomaly is that the metallic nickel phase appears to increase under oxidizing conditions. Note the appearance of Ni^0 at t=192 h for the C-5R and "SB" samples, where none was detected in identical samples removed from the then reducing atmosphere some 100 h earlier. The presence of the metallic nickel phase was observable with a bar magnet for those samples exhibiting strong metallic nickel spectra; however, the presence of terminal metallic nickel may be an artifact of the samples' prior reducing history. Observation of metallic nickel in a cathodically infused tile structure was noted in posttest analysis of a fuel cell.[6] Swaroop[6] reported the presence of metallic nickel in his cell analysis, but commented that this finding was thermodynamically questionable.

The SEM analysis of the sinters confirmed the XRD results. At all three firing temperatures--1200, 1400, and 1600°C--the C-70 based aluminate underwent the most dramatic change (erratic aggregate growth to >100 μm in 100 h and then apparent diminution thereafter) whereas the more monolithic

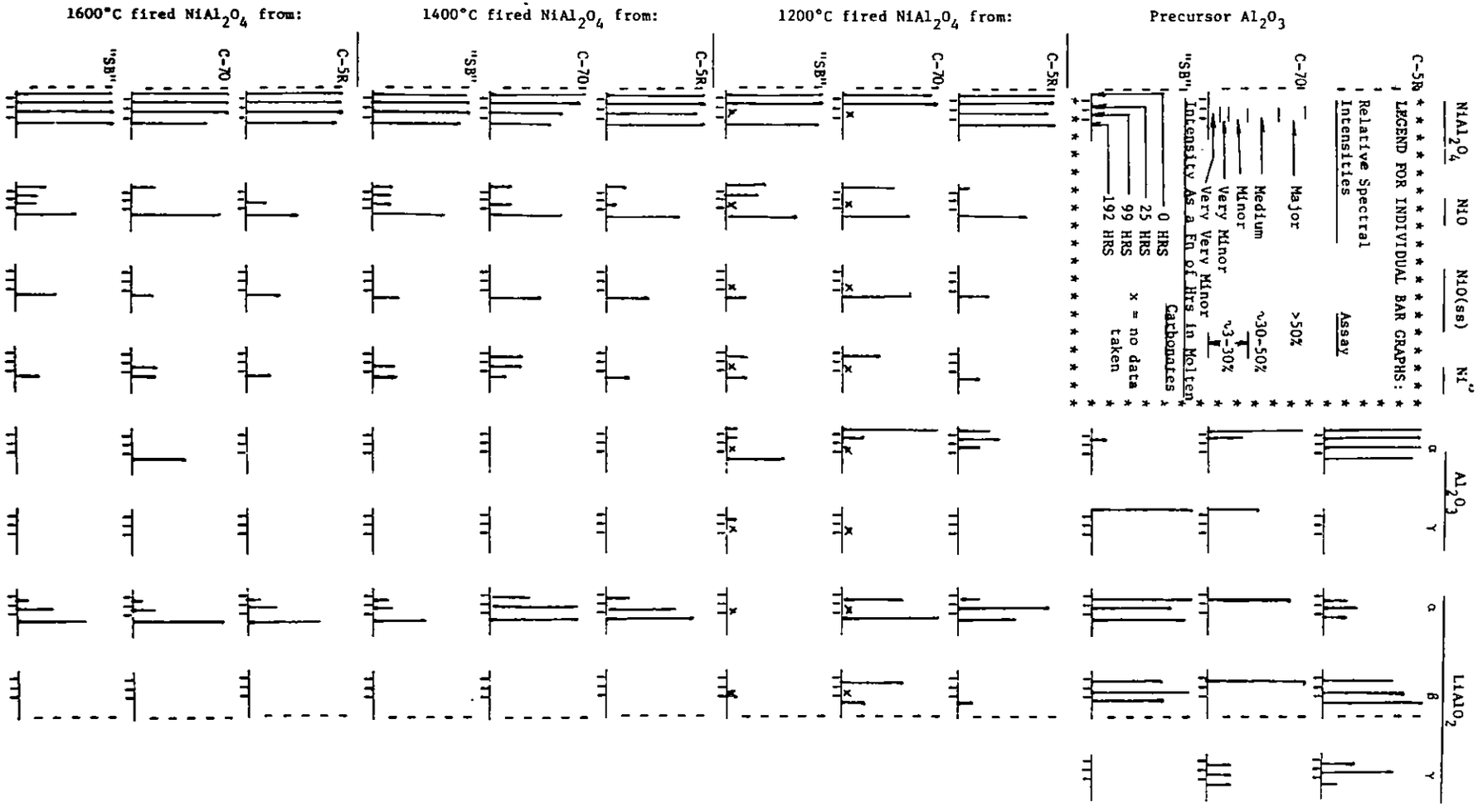

Fig. 7. Summary XRD Data Sheet for Changes in Composition of Nickel Aluminates and their Precursor Aluminas as a Function of Aging in Molten Li_2CO_3-K_2CO_3 at 650°C

C-5R and Catapal "SB" remained at the same size (5 μm). An interesting exception was the observation of long, tapered rods (15-μm long by 0.5-μm wide) that appeared in the 1600°C C-5R based sinter after 192 h. Figure 8 is a photomicrograph showing the shape of these needles, which, otherwise unidentified, appeared at the time the XRD data showed an increased (from minor to high-medium) intensity in the α-Al_2O_3 spectra.

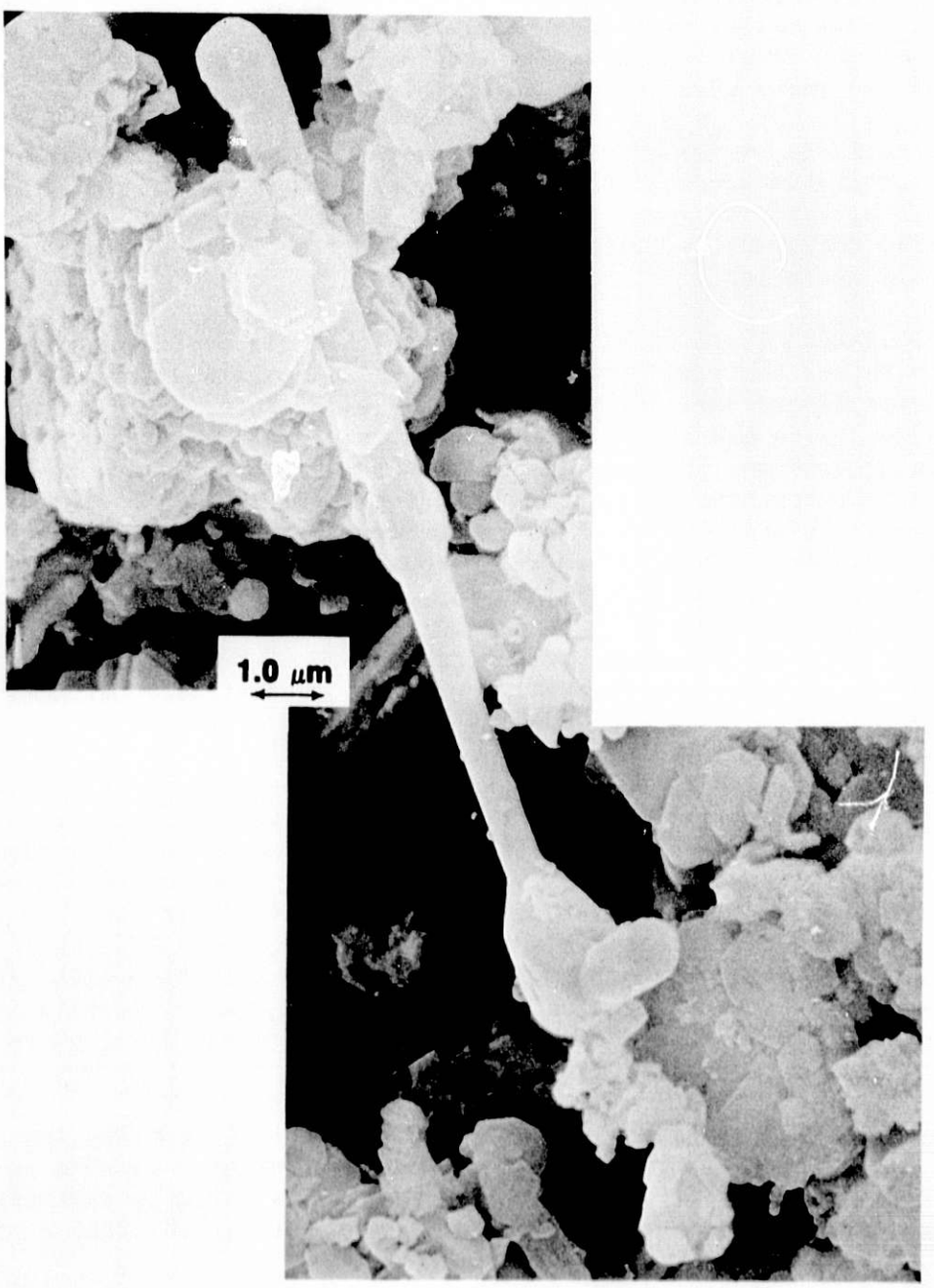

Fig. 8. SEM Photomicrograph of Acicular α-Al_2O_3 (?) Grown from $NiAl_2O_4$ in Molten Carbonate after 192 h at 925 K (ANL Neg. No. 308-81-195)

IV. CELL TESTING AND ANALYSIS
(J. L. Smith and J. R. Stapay)

A. Testing of Cell SQ-19

Cell SQ-19 was the first one to use a preoxidized, lithiated cathode (PC-6). The electrolyte structure was a hot-pressed tile of high-surface-area (~30 m^2/g) lithium aluminate and 62.5 wt % eutectic. A conventional anode was used. This cell's performance, 0.77 V at 80 mA/cm^2 and 0.57 V at 120 mA/cm^2, was lower than normally attained (0.89 V at 80 mA/cm^2 and 0.81 V at 120 mA/cm^2 for a good cell at comparable flow).

The cell was assembled so that the wet seals would be established during heat-up. This was accomplished by selecting components to give a slight clearance for both the anode and cathode. During heat-up the wet-seal area of the tile deformed, establishing the seals. The seals did not degrade during cell operation.

It is desirable to assemble cells such that all components are in good contact with one another. However, this was not possible for cell SQ-19 due to component dimensional irregularities. The greatest irregularity was in the cathode, which had ripples, was warped, and had a thickness variation in excess of 0.08 mm. Early cell performance was very low due to the resultant poor intercomponent contact. During the first 200 h of operation, a compressive deformation of the cell package was observed with the linear motion transducers. This deformation probably resulted primarily from the tile conforming to irregularities in the cathode. During the time that the deformation was observed, a corresponding improvement of cell performance was brought about by the improved intercomponent contact. After 200 h of operation, this improvement in cell performance essentially ceased in spite of an applied stress of up to 0.35 MPa (based on cell area).

Cell polarization tests showed an unusually large performance improvement (~26 mV at 80 mA/cm^2) with a rich oxidant, which indicates insufficient active cathode surface. Posttest examinations revealed that, as expected, the pores within the agglomerates were filled with electrolyte. However, the agglomerates were so large that most of the wetted surface area was not available for the electrochemical reduction of oxygen and CO_2; this condition caused the poor cell performance. Posttest examination also revealed that cathode-tile contact was good over only about 80% of the cathode area. While the tile had conformed partially, it was not pliable enough to accommodate the full cathode irregularities.

"Softer" tiles have been produced for future cell tests by increasing the carbonate content to 64 wt %. A cathode as irregular as that in SQ-19 may be accommodated with the softer tile, but it is unlikely that conformance can be achieved with dimensional irregularities greater than those of PC-6.

B. Posttest Microscopic (SEM) Examination of Cell Components
(J. W. Sim)

Pieces of the cathode and anode used in cell SQ-19 were examined by SEM to determine the extent of coverage of the pores by the carbonates. Both the cathode and anode were examined in cross-section, on the faces contacting the

electrolyte tile and on the faces contacting the current collector. For both the cathode and the anode, no obvious differences were observed from one face of the electrode to the other, suggesting that pore coverage is the same throughout the thickness of the electrodes. A piece of the porous cathode plate (PC-6) before cell testing also was examined for comparison with the plate after it had absorbed carbonates from the electrolyte tile. A typical anode before cell testing had been examined previously.

As shown in Figs. 9 and 10, the microstructure of the porous cathode plate (PC-6) before cell testing consisted of grains of lithiated NiO (about 0.5-1.0 μm) sintered together into agglomerates of about 35-50 μm. Within the agglomerates there were fine pores ranging in size from about 0.5 to 3 μm, and between the agglomerates there were coarse pores ranging in size from about 10 to 25 μm. In general, this bimodal pore distribution is desirable, as the fine pores within the agglomerates provide surface area for the electrochemical reactions, while the larger pores between the agglomerates provide channels for passage of reactant gases to the reaction sites. However, we suspect that the sintered cathode plate (PC-6) contained too much of its porosity in the fine pore (intra-agglomerate) range.

Microscopic examination of the cathode after testing in cell SQ-19 indicated that the grains within the agglomerates were coated with a film of carbonates (see Fig. 11), while the pores between the agglomerates were open and were not filled with carbonates (see Fig. 12). The grains within the agglomerates appeared to be larger after cell operation than before cell operation, and the surface texture of the grains was somewhat rougher after cell operation than before. The apparent increase in grain size during cell operation is probably not real, the carbonate film on the grain making the grain appear to be larger than it actually is. Our general conclusion from the posttest examination of the cathode is that the wetting of the cathode by the carbonates proceeded as desired, i.e., the large pores remained open for gas passage, while the fine pores within the agglomerates were well covered to provide surface area for electrochemical reaction. We suspect, however, that many of the fine pores were too deep within the agglomerates to provide effective reaction surface and that a cathodic structure with smaller agglomerates would be better.

The microstructure of a typical anode before cell testing consists of a network of sintered nickel-10% chromium grains (about 2-3 μm), with pores of about 3-8 μm between the grains, as shown in Fig. 13. After cell testing, the surface texture of the grains had become roughened, the grains appeared to be larger, and the pores between the grains were open for reactant gas passage, as shown in Fig. 14. Once again, the carbonate film on the surface of the grains probably made them appear to have increased in size. We believe that wetting of the anode by the carbonates was good. The surfaces of the nickel grains throughout the electrode were covered with a film of carbonates, providing surface area for electrochemical reaction, while the pores of the electrode were open for passage of the reactant gases.

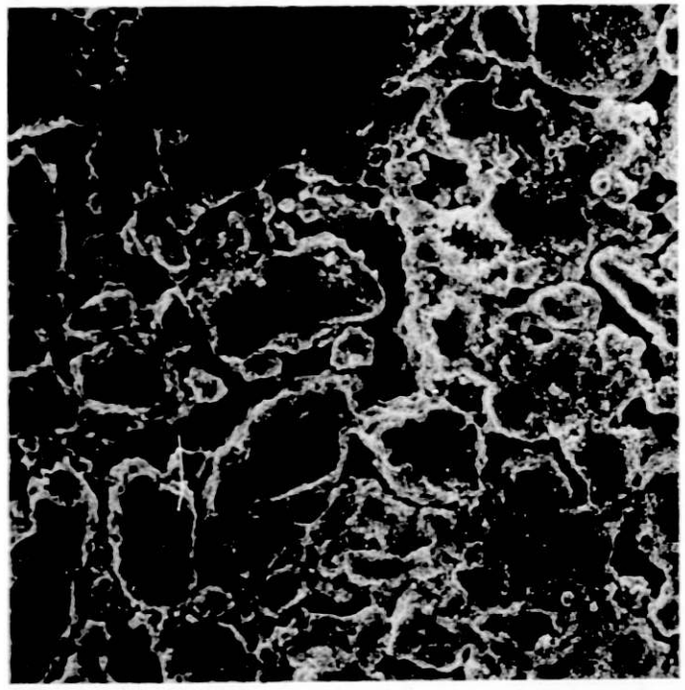

Fig. 9. Microstructure of Sintered NiO Cathode (PC-6) before Cell Testing Showing Fine Intra-agglomerate Porosity and Coarse Inter-agglomerate Porosity (ANL Neg. No. 308-81-196)

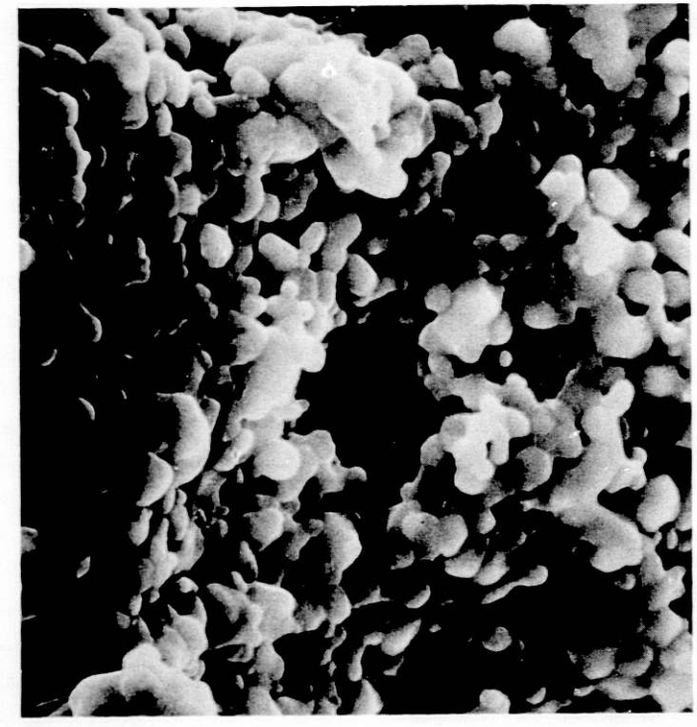

Fig. 10. Microstructure of Sintered NiO Cathode (PC-6) before Cell Testing Showing Fine Intra-agglomerate Porosity (ANL Neg. No. 308-81-197)

Fig. 11. Microstructure of Sintered NiO Cathode (PC-6) after Cell Testing Showing Carbonate on the Grains and in the Fine, Intra-agglomerate Pores (ANL Neg. No. 308-81-199)

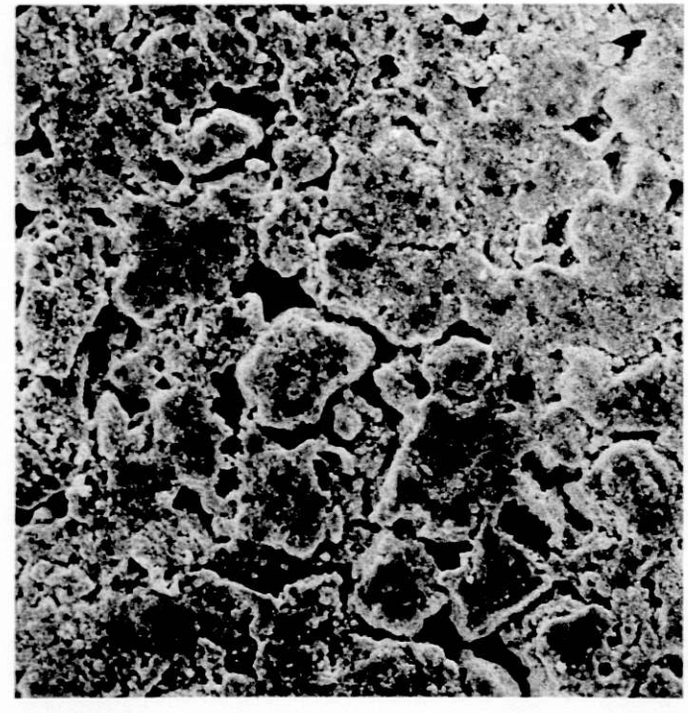

Fig. 12. Microstructure of Sintered NiO Cathode (PC-6) after Cell Testing Showing that Coarse Inter-agglomerate Porosity Remains Open (ANL Neg. No. 308-81-198)

Fig. 13. Microstructure of Typical Porous Sintered Nickel (10% Chromium) Anode before Cell Testing (ANL Neg. No. 308-81-200)

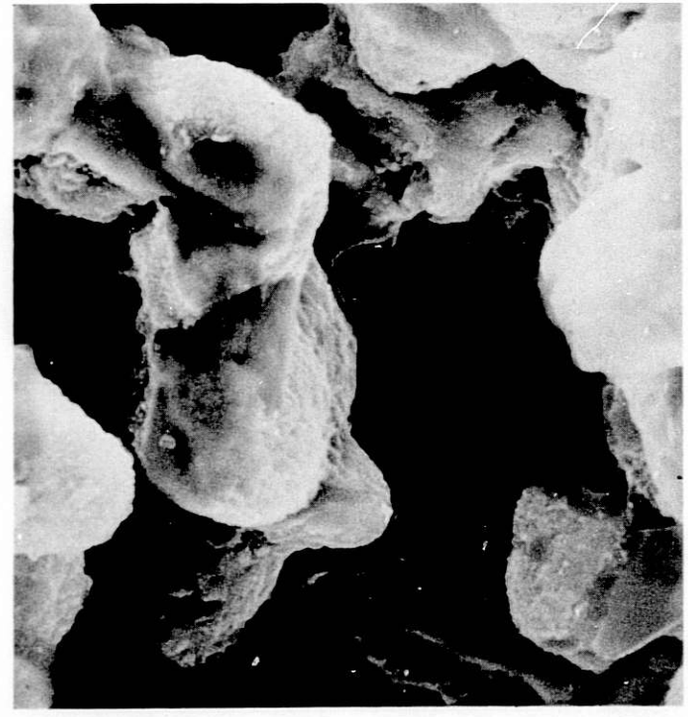

Fig. 14. Microstructure of Anode after Cell Testing in Cell SQ-19 Showing Coverage of Grains by Carbonates and Open Pores (ANL Neg. No. 308-81-201)

C. Cell Resistance Measurement
(J. L. Smith and J. R. Stapay)

The cell resistance for test cells is determined by current interruption. The bipolar transistor previously used for these measurements was switching in approximately 0.5 μs. In bench tests it gave a clean on-to-off transition. When it was used in a cell test, considerable high-frequency noise occurred during the first 1 to 3 μs. The on-to-off transition was, however, good enough for traditional IR measurements. The duration and magnitude of the noise was dependent on lead length, orientation, etc. It may be that what appears to be noise is a real effect of switching the cell in extremely short times. This possibility may be better understood through the use of an improved switch in conjunction with a high-speed digital storage oscilloscope.

The switching is now done with a vertical metal oxide semiconductor power field effect transistor (VMOS power FET), which is now operating with a clean on-to-off transition of 1-A current in 50 to 100 ns (see Fig. 15). In order that the switching time not be degraded, the switch will be connected to the cell with clamped flat conductors. Thus, cell current should be switched in 50 to 100 ns; if voltage fluctuations occur for about 3 μs as previously observed, they will have originated within the cell. The switch also will be used in a fundamental study of potential relaxation characteristics of molten carbonate fuel cells.

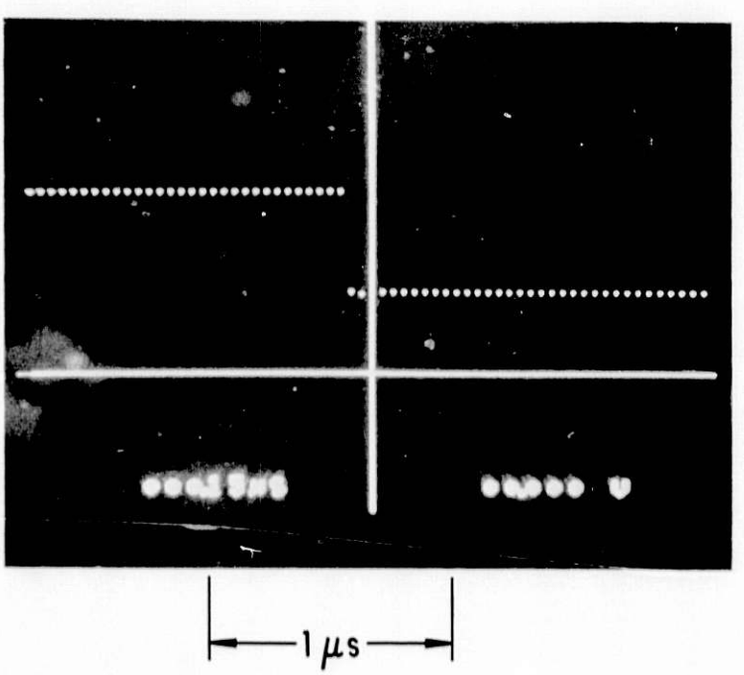

Fig. 15. Waveshape Created by Switching about 1/3 A with Mosfet Switch

REFERENCES

1. K. Kinoshita, J. W. Sim, and G. H. Kucera, Mat. Res. Bull. 14, 1357-1368 (1979).

2. Phase Diagrams for Ceramists, 1975 Supplement, E. M. Levin and H. F. McMurdie, eds., Am. Ceram. Soc., pp. 300-301.

3. H. R. Brownstein et al., Study of the Reaction Forming Lithium-Doped Nickel Oxide, 158th Electrochem. Soc. Meeting, Hollywood, FL (October 1980).

4. C. J. Toussaint, J. Appl. Cryst. 4, 292 (1971).

5. P. A. Lessing and J. J. Rasmussen, Characterization of Ceramic Materials for Use in Molten Carbonate Fuel Cells, Abstracts of National Fuel Cell Seminar, July 14-16, 1980, pp. 161-164.

6. J. P. Ackerman et al., Advanced Fuel Cell Development, Progress Report for January-March 1977, Argonne National Laboratory Report ANL-77-29, pp. 31-35 (June 1977).